25

A New Tool for Nonstationary and Nonlinear Signals: The Hilbert-Huang Transform in Biomedical Applications

Rui Fonseca-Pinto
School of Technology and Management
Polytechnic Institute of Leiria
Portugal

1. Introduction

Time-frequency techniques constitutes a major improvement in signal analysis, namely at the field of biomedical signals in which the interdisciplinary nature of the proposed questions implies the development of new strategies to answer to specific problems. Time-frequency analysis using Wavelets, Wigner-Ville transform and more recently the Hilbert-Huang Transform (HHT) constitutes the core of these tools with applications in biomedical signals in last years.

The non-linearity and non-stationarity nature of these signals puts HHT as a powerful tool to process signals with those properties, avoiding artefacts related to the use of linear and stationary assumptions.

Classical spectral analysis using Fourier Transform still the most commonly used method when one wants to measure the global power-frequency distribution (power spectrum) of a given signal.

In all areas of knowledge, Fourier-based analysis of time-series data faces constraining limitations. In biomedical signals, the critical constraining factors are the shortness of total data span, the non-stationarity of the data and the nonlinearity of the underlying physiological process.

Methods using Short Time Fourier Transform (STFT) are able to extract the spectral information by defining short time windows and locally computing the Fourier transform, thereby coping with non-stationary phenomena. The frequency resolution is inversely proportional to the window length, and changes in time resolution (window length) compromise the frequency resolution. Even with optimized joint time-frequency localization, the trade-off between time and frequency resolution is unavoidable.

In spite of these limitations, classical Fourier spectral analysis is still widely used to process biomedical data, for lack of alternatives. The uncritical use of Fourier spectral analysis and the careless adoption of the stationary and linear assumptions may give misleading results.

Wavelet theory developed in the 90's of last century was a significant contribution to tackle the problem of non-stationarity in time-series analysis. In common with Fourier-based analysis such as STFT, wavelet analysis yields a time-frequency representation, the main difference being that the decomposition is not based on sinusoidal functions, but rather

using a so-called "mother function", from which "daughter" wavelets are obtained by means of scaling procedures.
Nonetheless, wavelet theory is also limited by the fundamental uncertainty principle, according to which time and frequency cannot simultaneously be resolved with the same precision. The issue of non-linearity remains problematic. Besides, wavelet analysis entails the choice of the wavelet mother, and that choice may not be optimal for the time-series being studied.
The Hilbert-Huang Transform is a time-frequency technique whose philosophy is different from others, as the core of the technique consists in a signal decomposition *a posteriori*, enabling the extraction of the inner scales of each signal.
This chapter is meant to illustrate the potential of this technique by showing is performance in two applications in signal/image processing using medical data. The first example is about inner body regulation by autonomic nervous system. This is a classical topic in internal medicine, in which classical spectral techniques mostly had been used. For those interested in explore new techniques in these area, this chapter contains a state of the art in this subject and presents a new approach to this problem. The other application is an image feature extraction of lesion borders and artefact removal, based on 1D signal processing technique.
We start by reviewing some basic ideas of signal processing techniques, avoid as possible, strong mathematical notation.

2. Classical spectral analysis and new time-frequency methods

Spectral analysis using Fourier Transform (FT) is the most commonly used method when one wants to measure the global power-frequency distribution (power spectrum) of a given signal, forming a bridge between two spaces (time and frequency). This relationship is regulated by the Fourier Transform (FT) of a signal s defined by

$$S(f) = F\{s(t)\} = \int_{-\infty}^{+\infty} s(t) e^{-i\omega t} dt, \text{ where } \quad \omega = 2\pi f \tag{1}$$

and by Inverse Fourier Transform (IFT)

$$s(t) = F^{-1}\{S(f)\} = \int_{-\infty}^{+\infty} S(f) e^{-i\omega t} df \tag{2}$$

Equation (2) states that signal s can be expressed as the sum of complex exponentials of different frequencies, whose amplitudes are the complex quantities $S(f)$ defined by (1). In practice the frequency content is usually represented as the magnitude squared of (1); $|S(f)|^2$.
In all areas of knowledge, Fourier-based analysis of time-series data faces constraining limitations. In biomedical signals, the critical constraining factors are the shortness of total data span, the non-stationarity of the data and the nonlinearity of the underlying physiological process.
Methods using Short Time Fourier Transform (STFT) are able to extract the spectral information by defining short time windows and locally computing the Fourier transform, thereby coping with non-stationary phenomena.

The frequency resolution is inversely proportional to the window length, and changes in time resolution (window length) compromise the frequency resolution. Even with optimized joint time-frequency localization, the trade-off between time and frequency resolution is unavoidable (Gabor D, 1993).
In spite of these limitations, classical Fourier spectral analysis is still widely used to process biomedical data, for lack of alternatives. The uncritical use of Fourier spectral analysis and the careless adoption of the stationary and linear assumptions may give misleading results (Huang N et al., 1998).
Wavelet theory developed in the 90's of last century (Daubechies I, 1988; Daubechies I, 1992; Meyer Y, 1993) was a significant contribution to tackle the problem of non-stationarity in time-series analysis. In common with Fourier-based analysis such as STFT, wavelet analysis yields a time-frequency representation, the main difference being that the decomposition is not based on sinusoidal functions, but rather using a so-called "mother function", from which "daughter" wavelets are obtained by means of scaling procedures.
Nonetheless, wavelet theory is also limited by the fundamental uncertainty principle, according to which time and frequency cannot simultaneously be resolved with the same precision. The issue of non-linearity remains problematic. Besides, wavelet analysis entails the choice of the wavelet mother, and that choice may not be optimal for the time-series being studied.
Recently Huang and its co-workers developed a method in which the issue of non-linearity is treated, by using a procedure to decompose the signal according to its own scale properties. This method enables to obtain for each signal a set of orthogonal functions, i.e. a set of a basis functions. It is a data driven and *a posteriori* method, contrasting with other class of decompositions, whose basis functions are established *a priori* (trigonometric functions, and wavelets) and in the former case with constant amplitude and frequency (sinusoidal functions). This method proposed by Huang in 1998 (Huang N.E et al 1998) is known by Hilbert-Huang Transform (HHT) comprise two parts, the EMD – Empirical Mode Decomposition, and the Hilbert Spectral Analysis (HSA).

2.1 Short Time Fourier Transform – STFT

The strength of classical Fourier analysis is that it allows the decomposition of a signal into its individual frequency components and establishes the relative intensity of each frequency component. Due to the infinite durations of these basis functions, any time-local information is spread over the whole frequency spectrum.
To overcome the time localization issue, Gabor introduced a sliding window to well localize variations in time domain. This procedure is known by Short Time Fourier Transform – STFT. When the applied window follows a Gaussian shape, this STFT is also called Gabor Transform.
Similar to the FFT case, the magnitude squared of STFT is used in practice (the spectrogram), giving now information as a function of time and frequency, and is define by

$$S(t,f)=\left|\int_{-\infty}^{+\infty} s(\tau)h(t-\tau)e^{-i\omega\tau}d\tau\right|^2 \tag{3}$$

The major advantage of STFT is that if a signal has most of its energy in the interval $[-T,T]$ and in the frequency range $[-\omega,\omega]$, then its STFT will be localized in the region

$[-T, T] \times [-\omega, \omega]$ in the time-frequency plane. The uncertainty principle prevents de possibility of having arbitrary high resolution in both time and frequency domains, since it lowers-bounds the time bandwidth product of any basis function by $\Delta T \Delta \omega \geq 1/4\pi$, where $(\Delta T)^2$ and $(\Delta \omega)^2$ are the variances of time function and its Fourier Transform respectively.

2.2 Wavelet Transform – WT

Wavelet Transform (WT) mitigates the limitations of FT and STFT by having a basis function which can be both shifted and dilated or contracted. By decomposing the time-scale plane, WT enhances time and frequency domains representation of signals, as is the first proposed method comprises an adaptative nature.

WT[1] of a signal s is expressed as

$$C(a,b) = \int s(t) \overline{\varphi}_{a,b}(t) dt \tag{4}$$

Where $\overline{\varphi}_{a,b}(t)$ is defined as,

$$\overline{\varphi}_{a,b}(t) = \frac{1}{\sqrt{a}} \overline{\varphi}\left(\frac{t-b}{a} \right) \tag{5}$$

In (4) $C(a,b)$ are the wavelet coefficients. $\overline{\varphi}(.)$ is known as the mother wavelet, and $\overline{\varphi}_{a,b}(.)$ is its stretched and translated version with a and b as its scale and translation parameters.

For a detailed explanation about WT is possible to find several references, in particular Daubechies, 1992 and Addison P, 2002, among other good books.

2.3. Hilbert-Huang Transform - HHT

The Hilbert-Huang transform is a time-frequency technique consisting of two parts. In the first part, EMD the signal is decomposed into Implicit Mode Functions -IMF's, putting forward the scale characteristics imbedded in the signal. In the second part, the Hilbert transform is applied to the IMF's, yielding a time-frequency representation (Hilbert spectrum) for each IMF.

HHT has been applied to different fields of science since is first application to fluid dynamics in water waves and ocean engineering (Ding et al., 2007; Rao & Hsu, 2008), financial applications (Huang N et al., 2003), system identification (Xun & Yan, 2008; Quek T et al, 2003) medical signals (Tang J. et al., 2007; Salisbury & Sun, 2007; Caseiro P. et al., 2010). By it's owns characteristics biomedical signals are indicated to HHT analysis.

An IMF is a function that satisfies two conditions:

1. in the whole data set, the number of extrema and the number of zero crossings must either be equal or differ at most by one;
2. at any point, the mean value of the envelope defined by the local maxima and the envelope defined by the local minima is zero.

Unfortunately, most time-series do not meet these criteria. At any given time, the data may involve more than one oscillatory mode. This is the reason why the simple Hilbert Transform cannot provide the full description of the frequency content in general data

1 In fact, CWT for, Continuous Wavelet Transform.

(Cohen L, 1995). Thus, it is necessary to extract the oscillatory modes (IMF's) from the data, by means of the EMD procedure, which is implemented by an algorithm comprising the following steps:

1. Identify all extrema of $x(t)$;
2. Interpolate between minima to obtain the lower envelope $x_L(t)$, and between maxima to obtain the upper envelope $x_U(t)$;
3. Calculate the average envelope $e(t) = \frac{x_L(t) + x_U(t)}{2}$;
4. Extract the intrinsic oscillatory mode $d(t) = x(t) - e(t)$;
5. Iterate on the residual $e(t)$.

In practice, the above procedure has to be refined by first iterating steps 1 to 4 upon the detail signal $d(t)$, until the latter can be considered as a zero-mean signal according to some stopping criterion (Huang et al, 1998). In Figure 1 at left, is possible to verify that after first iteration of this shifting procedure, the signal do not achieve the two conditions for IMF. After a set of iterations (varying within different signals) the zero mean is reached and the first mode of oscillation is them achieved, as is possible, as is possible to observe in Figure 1 at right.

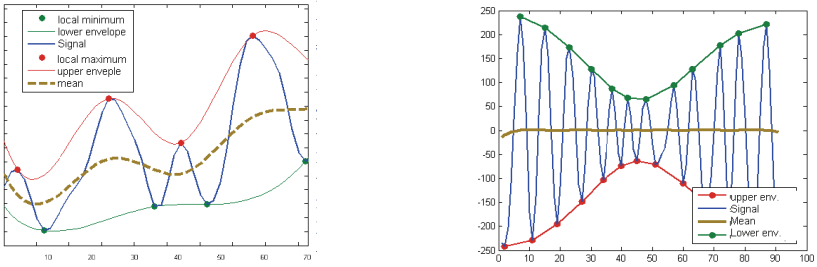

Fig. 1. Left – first iteration of shifting. Right - first IMF after several iterations

Interpolation in step 2 is made using cubic splines; however other interpolation techniques may be applied (Long SR et al, 1995). The aim of this repeated operation is to eliminate the riding waves and to achieve more symmetrical wave-profile by smoothing the uneven amplitudes. Once this is achieved, the detail is considered as the effective IMF, the corresponding residual is computed and step 5 follows. An example of a EMD decomposition is presented in Figure 2, were the signal is in the first row, giving in this case 5 oscillatory intrinsic modes (or scales) of oscillation.

Having obtained the IMF's components, it is possible to apply the Hilbert Transform (HT) to each component, to get instantaneous frequency.

The HT of a real signal $x(t)$ is defined as

$$H[x(t)] = x * \frac{1}{\pi t} = y\,, \tag{6}$$

or using the convolution definition,

$$y(t) = \frac{1}{\pi} P \int_{-\infty}^{\infty} \frac{x(\tau)}{t - \tau} d\tau \tag{7}$$

where P indicates the Cauchy principal value. From $y(t)$ it is possible to define the analytical signal $z(t) = x(t) + iy(t)$ or, in polar form, $z(t) = a(t)e^{i\theta(t)}$, in which

$$a(t) = \sqrt{x^2(t) + y^2(t)}\ , \quad \theta(t) = \arctan\left(\frac{y(t)}{x(t)}\right). \tag{8}$$

Instantaneous frequency is defined using the instantaneous variation of phase,

$$\omega = \frac{d\theta(t)}{dt} \tag{9}$$

This is the second part of the HHT (Hilbert spectral analysis, HSA), and it entails writing the signal in the form

$$x(t) = \sum_{j=1}^{n} a_j(t) e^{i\int \omega_j(t)dt}. \tag{10}$$

We can thus obtain the amplitude and the instantaneous frequency as a function of time $H(\omega, t)$. This time-frequency representation is called the Hilbert Spectrum (HS). This spectral representation offers a totally different interpretation when compared to the classical Fourier representation. In Fourier terms, the existence of energy at some frequency implies the existence of a component of a sine or a cosine wave throughout the whole time-series or a significant part of it. A time-frequency technique allows for the extraction of the frequency content at each time point. The HS of the signal whose decomposition is in Figure (2) is presented in Figure (3)

To obtain a measure of the total amplitude (or energy) contribution from each frequency value, we can compute the Marginal spectrum defined by

$$h(\omega) = \int_0^T H(\omega, t)dt. \tag{11}$$

Similarly it is possible to achieve a measure of the energy of the signal with respect to time, if we compute the Instantaneous Energy Density Level, IE defined by

$$IE(t) = \int_{\omega} H(\omega, t)^2 d\omega. \tag{12}$$

As already reported elsewhere in the text, the uncritical use of Fourier derived techniques may lead to the extraction of ambiguous information from the data, and in other cases, may lead to failure to extract properties and characteristics of the signal. The use of HHT allows for a decomposition of the signal that resorts to an adaptative set of basis functions. It is therefore possible to use HHT without a predefined choice of parameters.

3. Time-frequency analysis in biomedical signals: applications

In this chapter two examples of HHT applications are shown. The first in the field of Sympathovagal balance (SVB) and the other uses digital images of the surface of the skin (dermoscopic images).

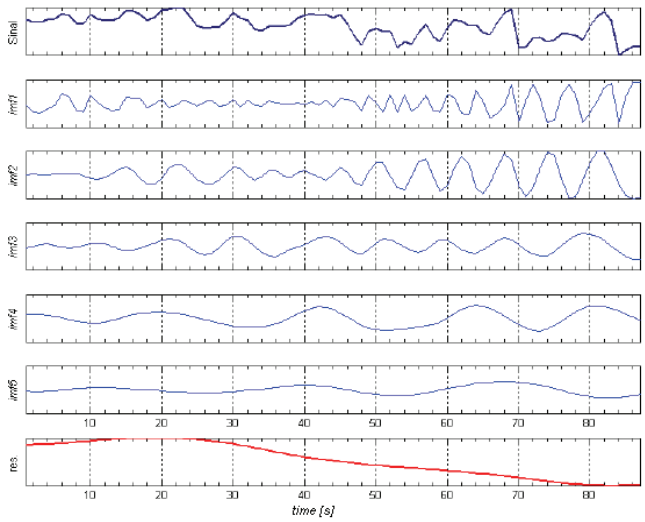

Fig. 2. Signal (first row) and EMD decomposition plus trend or residue (in last row)

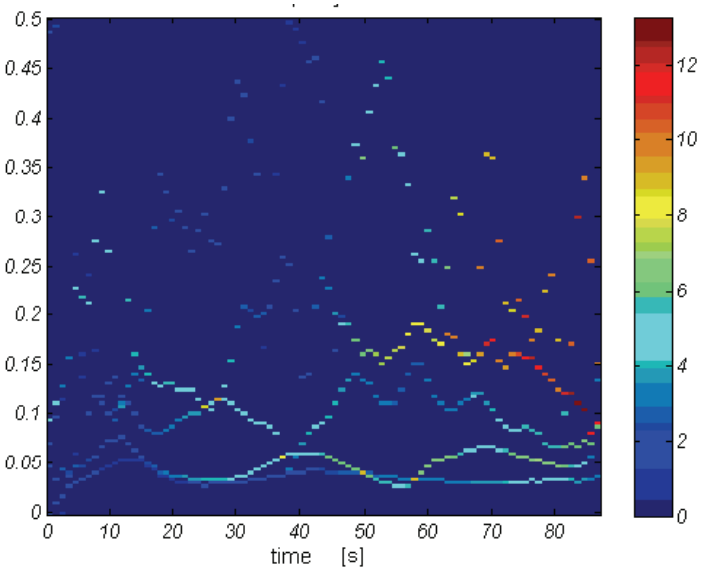

Fig. 3. Hilbert Spectrum of the signal whose decomposition is in Figure 2

3.1 Sympathovagal Balance – SVB

The Nervous System (NS) is one of the human body systems enrolling more complexity, whose interactions among others systems are yet partially unknown. Discovering how it behaves, and is complex relationships within the whole body, is still a major challenge for those who are interested in understanding how the human body really works.

The Autonomic Nervous System (ANS) is a breach of the Peripheral Nervous System (PNS). The ANS is a neural network suitable to regulate cardiovascular function and work at a subconscious level by regulating visceral functions. The main function of the ANS is control cardiac output and blood supply at central and peripheral levels. Cardiac output is controlled by ANS and is modulated by its main components: Sympathetic Nervous System (SNS) and Vagal System[2] (VS).

The variation in Heart Rate (HR) is defined as the variability of the time-series of heart beats, and is called Heart Rate Variability (HRV). Epidemiological Studies showed that a decrease in HRV is one of the best predictors of arrhythmic events and sudden death after myocardial infraction.

One way to study cardiovascular neuronal regulation is to perform a spectral analysis of heart rate variability and blood pressure signals. Usually, spectral procedures are designed to separate the full spectrum of the signal into two main frequency bands associated with vagal and sympathetic subdivisions of the autonomous nervous system.

Regulation of blood pressure is a continuous phenomenon. Short term adaptation is mainly dependent on sympathetic outflow to arterial muscle, and largely controlled by baroreflexes. Changing from supine to upright position leads to gravitational dependent pooling of blood in dependent parts, namely legs, distal portion of arms and venous abdominal plexes, thereby reducing ventricular feeling, cardiac output and blood pressure. Blood pressure lowering is sensed by baroreceptors in carotid bodies, giving rise to a reflex mediated by sympathetic activation, which determines arterial vasoconstriction and cardiac acceleration (Joyner M & Shepherd J, 1997; Shepherd R & Shepherd J, 1988).

Provocative manoeuvres can be used to evaluate autonomic vagal and/or sympathetic outflows indirectly. With these approaches, autonomic behaviour is inferred from measurements of cardiovascular variables. The analysis of heart rate and blood pressure variability applying Fast Fourier Transform (FFT) and autoregressive (AR) spectral analysis to these signals has made a very important contribution to autonomic evaluation (Ducla-Soares JL et al, 2007).

Heart rate varies during inspiration and expiration[3]. The most evident fluctuations of HR are related to respiration and manifest as increased HR during inspiration and decreases HR during expiration (Hales, 1735). It has been clearly shown that a linear relationship exists between heart frequency and vagal activity. The influence of the ANS has been recognized in HR short-term variability and is mediated by vagal system. Experimental data has clearly shown that vagal activation slows heart rate and inversely, vagal block determines heart rate increases (Freeman R, 1997).

The direct quantification of vagal activity in humans is difficult as recording directly from the nerve is highly invasive. The degree of RSA provides a quantitative measure of the vagal outflow to the myocardium, since RSA is generated by cardiac vagal nerve traffic. Spectral analysis techniques have been applied to HRV in order to estimate the frequency component centred about the respiratory frequency, termed high frequency band (HF) of the spectrum (0.15 Hz – 0.4Hz). In studies whose experimental conditions may vary the respiratory frequency, the value of this central frequency constitutes crucial information. For

[2] Also known by Parasympathetic Nervous System (PaNS).

[3] The influence of respiration in HR has been known for more than one century and is called Respiratory Sinus Arrhythmia (RSA).

instance, breathing at slow frequency, as is the case during deep breathing manoeuvre[4] at 6 cycles per minute, heart frequency oscillations fall in the low frequency (LF) part of the power spectrum. In HRV data is also possible to find a lower frequency component centred around 0.1 Hz, related to the Meyer Waves[5] and baroreceptors.
Spectral analysis of HRV data also shows a Low Frequency band (0.04 Hz-0.15Hz), which physiological significance is more difficult to establish, as the pharmacological blockage in vagal activity also produce reduction in LF power. Some researchers have being settled that LF variability may have a vagal and sympathetical component and therefore they state that LF is not a pure measure of sympathetic activity (Akselrod et al, 1985; Malliani et al, 1991; Eckberg, 1997). Other studies indicate that LF[6] represents the primary sympathetic modulation of heart rate. The ratio LF/HF is defined as the Sympathovagal balance (SVB) (Pagani et al, 1986; Malliani et al, 1991).
Behind the two above mentioned LF and HF frequency bands, RR interval power spectrum can present also two more bands, the Very Low frequency band (VLF) and the ultra low frequency band (ULF) whose spectral densities can be reliably analysed from long-term recordings (more then 18 hours).

3.1.1 Review of classical spectral methods to obtain SVB: a physiological and technical challenge

HRV time-series (RR intervals) is obtained form ECG data using algorithms designed to detect the QRS complexes, and time between R waves. Before trying to detect the R waves, the ECG signals are detrended using a locally weighted robust regression algorithm. Usually a vertical and horizontal threshold are established (the former to define a level that R wave must exceed, and the later to prevent detecting an R wave for a period of time after one was detected).

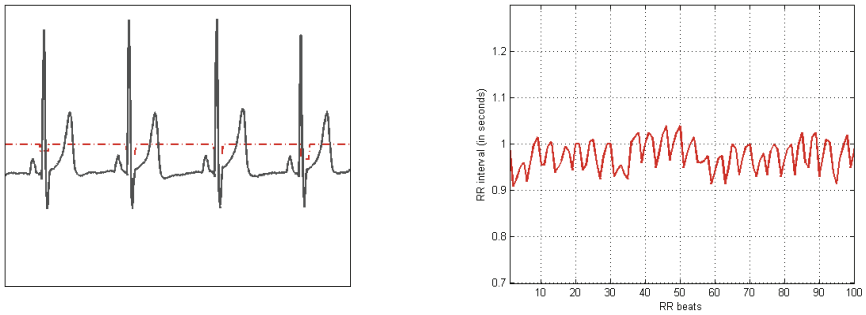

Fig. 4. Left – ECG and QRS detection. Difference in time between R waves plotted as a function of the RR beats is the tachogram, presented at right

[4] This is a autonomic test in which the subject is instructed to breath deeply at a rate of 6 breaths per minute, paced by a metronome (deep metronomic breathing). This and head-up-tilt test are the most commonly used strategies to standardize respiratory changes and their relation to heart rate, hence to vagal activity.
[5] Slow waves at one cycle in 10 seconds associated with sympathetic activation.
[6] In particular the ratio LF/(LF+HF), which is the normalized LF power.

After R waves identification, the HRV is calculated as the difference in time between RR waves (see Figure 4 at right). This information in time units, plotted as a function of the RR beats is known in the literature by tachogram.
The simplest form to extract information from a time-series is the inspection in time domain. By using time domain methods, is possible to calculate HR in any point, or intervals between successive normal ECG complexes, as well other statistic measures (NN intervals[7], RMSSD[8]) obtained from direct measures of HR or by differences between NN intervals. In time domain is possible to use also geometric models. More details about time-domain methods can be fund in (Malik, 1996).
RR signal represents de heart period at discrete points, but this representation is no suitable for FFT analysis as these points are not equally spaced. In order to produce RR data suitable for classical spectral analysis, the RR signal must be interpolated and re-sampled at higher uniform rate, usually at 2 or 4 Hz (Carvalho J et al., 2003).

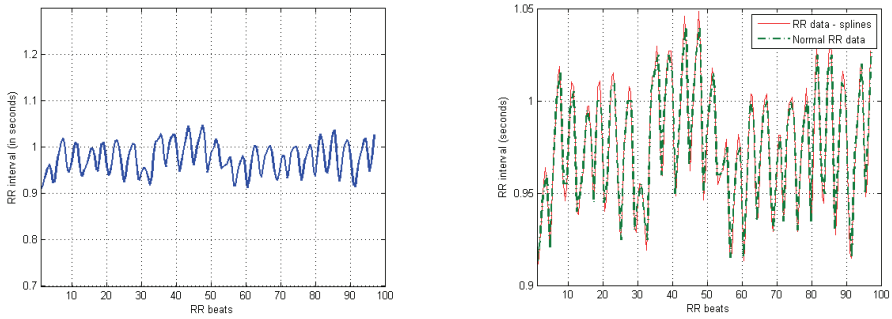

Fig. 5. Left – RR time-series after interpolation by cubic splines. In the right both signals are presented (before and after interpolation)

Parametric autoregressive modelling (AR[9], ARMA[10]) and nonparametric Fourier Transform methods (e.g. DFT[11]) provide classical frequency-domain methods to analyse HRV from RR interpolated signal.
Parametric methods by AR models uses linear prediction defined as

$$\hat{s}(k) = \sum_{i=0}^{p} b_i w(k-i) - \sum_{i=1}^{p} a_i s(k-i) \tag{13}$$

where s is the signal, a and b are prediction parameters and $w(k)$ white noise.
Non parametric spectral methods using DFT are usually implemented by an algorithm for fast computation of the DFT, which uses a recursive algorithm known by Fast Fourier Transform – FFT. The spectrum visualization in AR models is usually smoother then Fourier based ones (see Figure 6). In order to approximate results obtained form AR models from those obtained by FFT, the order of the AR model must increase. To get a good spectral

[7] Intervals between adjacent QRS complexes.
[8] Squared root of the mean squared differences of successive NN intervals.
[9] Autoregressive Model.
[10] Autoregressive Moving Average.
[11] Discrete Fourier Transform

estimation we must use order 12 in AR model for a sampling rate of 2Hz, and order 15 for a sampling rate of 4Hz (Carvalho J et al, 2003).

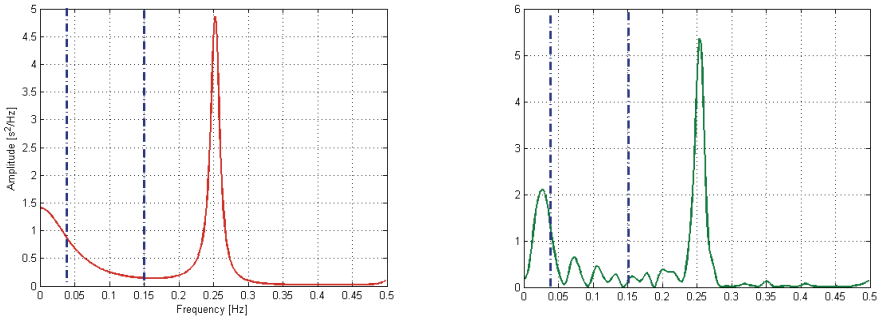

Fig. 6. Spectral analysis of RR signal in figure 2. Left: using AR model order 12. At right is present the spectrum of the same signal using FFT with an Hamming window

Using the HRV data from Figure 5 and spectral analysis in Figure 6, is possible to see a bigger energy input from high frequency band (0.15 Hz – 0.4 Hz), whose main frequency is 0.25Hz showing the RSA enrolment in HF band, representing the contribution of the Vagal System during this period of 100 heart beats.
The classical spectral analysis presented above, were designed for whole signal, abolishing time information. Form Figure 6 we just know that a wave of frequency around 0.25 Hz persist in all signal, lacking the time information. This required information of frequency in time is not possible using the classical frequency definition. Instead, an instantaneous frequency definition is required, being this one of the main characteristics of time-frequency analysis.
Behind the non-consensual physiological interpretation of LF frequency band, classical methods possesses these constrains related with lack of time guidance.

3.1.2 Access to SVB by HHT

The access to Sympathovagal Balance is an interdisciplinary problem, and in last years had been treated within research groups with Mathematicians, Engineers, Doctors and Medical Staff, see as an example the Guidelines of Task Force of The European Society of Cardiology and The North American Society of Pacing and Electrophysiology. Nevertheless the interdisciplinary nature of the panel, those guidelines was stated in 1996, lacking time-frequency techniques.
Today powerful techniques of time-frequency analysis were used by engineers to process data from all knowledge areas, as is the case of medical signal processing. Instantaneous frequency is defined mainly using the Hilbert Transformation (HT), and time-frequency techniques from different classes (atomics and energy) are today completely established. From STFT, WT and Wigner- Ville Transform (WVT) is possible to use numerous variants. HHT – Hilbert-Huang transform presents good skills to process these kind of data, diverging from the previous time-frequency techniques by lacking for an yet complete analytical formulation. This was the case regarding WT in the 80's of the last century, when a French mathematician *Ingid Daubechies* completed the Wavelet theory.
Using those recent time-frequency representations, new approaches had been proposed to process RR data in spectral domain, by using points sampled synchronously with each

heartbeat. By this way, frequencies are expressed in 1/heartbeat units. Working with frequencies (in Hz) is possible, but it would require re-sampling and interpolation procedures that may be problematic in high variability signals such as these (Fonseca-Pinto et al, 2010).

As we presented before, the algorithm enrolled the first part of the HHT (Empirical Mode Decomposition) behaves like a filter bank (Flandrin P, 2004), and this allows the separation of the spectrum in two main frequency bands (high frequency band, HF, and low frequency band, LF) without a predefined cut-off frequency. In order to study the modulation of the sympathetic nervous system activity, signals of Diastolic Blood Pressure (DBP) and Heart Rate Variability (HRV) were obtained following a protocol to extract values of DBP and HRV at each heartbeat (RR interval). These signals were obtained during the head-up tilt test and deep breathing manoeuvre, following the same procedures as in (Ducla-Soares J L et al 2007). In the former test, distinct postural positions are studied, including a 60-degree tilt of the bed where the subject is resting. In the latter test, the subject is instructed to breath deeply at a rate of 6 breaths per minute, paced by a metronome (deep metronomic breathing). This is one of the most commonly used strategies to standardize respiratory changes and their relation to heart rate, hence to vagal activity.

In the method presented next, DBP signals were used to access the Sympathetic modulation of SVB, and the HR signal is used to follow vagal output. By this formulation the SVB is constructed based in two signals (main indirect measures to access SVB), allowing a more realistic picture of the complex interactions performed to obtain homeostasis. DBP also reflects the vasoconstriction and is more sensitive to pressure changes.

Methods

The first step to achieve the separation in two frequency bands is to normalize[12] the HRV and DBP signals and to submit them to the EMD procedure. As stated before, in the present study we presented a new formulation by assigning the highest frequency modulation to the IMF1 of the heart rate signal, and the lowest frequency modulation to the sum of IMF2 and IMF3 obtained from the diastolic blood pressure signal as

$$x_{HF} = IMF_1(HR) \quad , \quad x_{LF} = IMF_2(DBP) + IMF_3(DBP). \tag{14}$$

As the number of IMF's is not a constant within different signals, in those cases with only two IMF's, the lower frequency content is obtained just considering the IMF2 from DBP.

This reconstruction in modes leads to a spectrum separation in two frequency bands. By this way it is possible to reproduce the two main frequency bands (LF and HF) related respectively with sympathetical system and vagal system used in studies with FFT and Wavelets (Parati G et al., 1995; Ducla-Soares J L et al., 2007). In the case of deep breathing, the highest frequency content is obtained from the IMF2 of the heart rate, considering the shift in heart rate towards the LF band, already mentioned and reported in (Sleight & Casadei, 1995).

The next step is the computation of the Hilbert spectrum associated with the high frequencies $H_{HF}(\omega,t)$, and the low frequencies $H_{LF}(\omega,t)$. For each case, a two-dimensional representation of the energy fluctuation with time is obtained (see equation (15)):

[12] Signals are divided by the maximum value of each one.

$$PS_{HF} = \int_{\omega} H_{HF}(\omega,t)^2 d\omega\,; \qquad PS_{LF} = \int_{\omega} H_{LF}(\omega,t)^2 d\omega \tag{15}$$

By considering a time range that is adequate from the point of view of the experiment (e.g. 5 heartbeats before and after the tilt), it is possible to calculate the energy contribution in function of time, related to the LF band and to the HF band, by computing IHF, ILF and Index defined by

$$IHF = \int_0^T PS_{HF} dt; \quad ILF = \int_0^T PS_{LF} dt; \quad Index = \frac{ILF}{IHF}. \tag{16}$$

Studies to evaluate the Sympathovagal balance involve postural manoeuvres, and it is critical to pinpoint fluctuations that happen synchronously with postural changes, or shortly before or after them. If the above time range is small when compared with the duration of the test, a better sensitivity to energy variations can be achieved.
Related to the issue of critical data length, simulation studies were carried out in order to understand the influence of the signal length in the number of IMF's produced by EMD. These recent studies were made using was made using fGn (fractional Gaussian noise) signals, and allowed to define a measure to establish the minimum data length needed to obtain a predetermined number of IMF's. In this proposed methodology, it is crucial that the number of IMF's are at least three (or two in some cases) in order to obtain the meaningful separation of frequency content, as explained above. According to previous simulation studies (Fonseca-Pinto R et al, 2009), to obtain 2 or 3 IMF's, the average number of signal samples required is 36 (RR beats).
The Hilbert-Huang Spectrum was obtained following Matlab™ routines adapted from (Rilling G, 2003). These routines contain functions of the TFTB (time-frequency) toolbox (Auger F, 2009).

Results

As a first example of the access to SVB using this HHT formulation we present in Figure 7 the HR and DBP signals from a period of 42 heart beats. In this registration is possible to observe a slow variation in DBP at the beginning (between 10th and 20th heart beat), and a more effective variation in HR increasing is variation mainly at the end of the record. In the same figure at right, we can track in time the energy fluctuation of the two frequency bands. Figure 8 at right show a prominent contribution of vagal system mainly after the 33rd heart beat period were HR decreases. In the period between 10th and 20th heart beat, HR increases and is possible to observe a decrease in vagal output and an bigger sympathetic input by improve $PS_{DBP.}$
In fact, this time-frequency derived technique by HHT, when compared with the classical representation presents greater advantages. To compare both spectra we present the classical spectral representation in Figure 6.
In fact, using Figure 8, all above local interpretations were impossible. We just are able to say that HF spectrum and LF spectrum present similar contribution, as the area above the curve for the two main frequencies roughly is similar. In fact the LF/HF ratio is in this case bigger than one. It is also important here to register that in the HHT based method the LF spectrum is obtained for a different signal (DBP) and by this way is impossible fully compare both spectra.
Another example is showed in Figure 9. In this sketch is possible to observe at right both signals of HR and DBP during 50 heart beats.

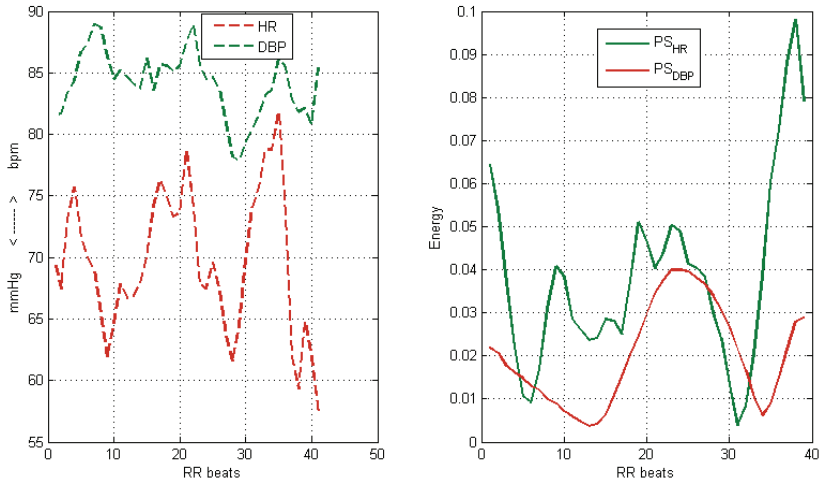

Fig. 7. SVB by HHT- left: HR and DBP signals –Right: Instantaneous Energy fluctuation of Vagal and Sympathetic systems

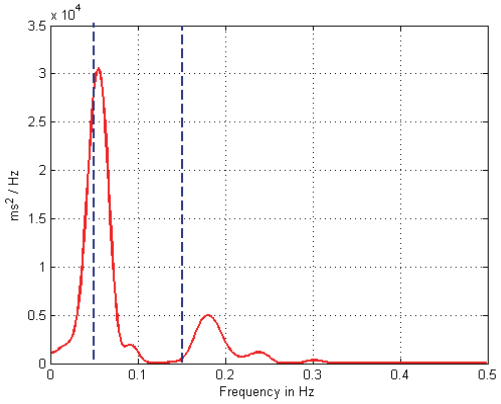

Fig. 8. Classical Spectrum of HR signal in figure 5. Vertical dashed lines mark LF (0.04Hz-0.15Hz) range

During the firsts 20th heart beats we assist at an increase in HR and a decrease in DBP. In fact, during almost all record, DBP possesses a descendent behaviour. This initial deed of HR is elucidated in the figure at right by an SVB (LF/HF) bigger than unity. Actually in this period the vagal system varies slowly. At the end (between 40th and 50th heart beat) DBP increases and HR decrease and once more SVB is bigger than one. In fact we assist variability in DBP conducted by an Sympathetical inflow. This is enhanced by the fact that HR continues is descending path, hence vagal system contribution in insufficient to balance LF component.

As we do previously the classical spectrum is also presented in Figure 11. In this case we also use other time-frequency method to be able to compare two time-frequency methods.

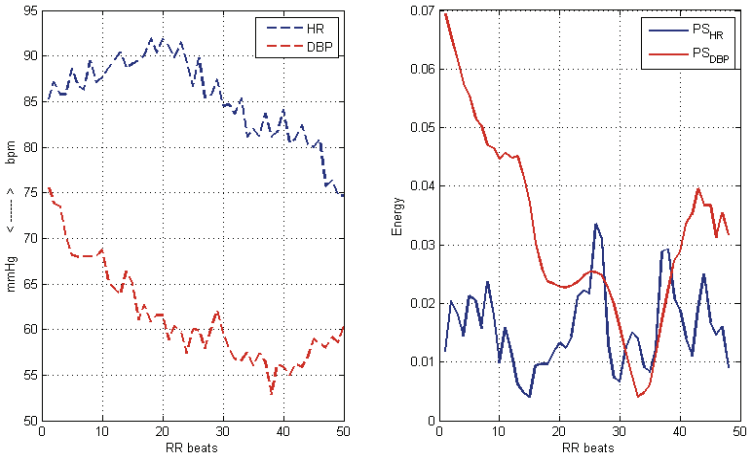

Fig. 9. SVB by HHT- left: HR and DBP signals –Right: Instantaneous Energy fluctuation of Vagal and Sympathetic systems

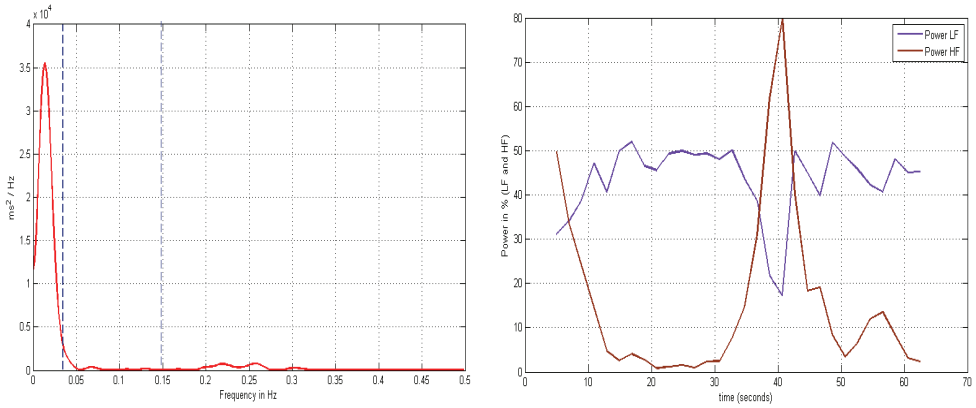

Fig. 10. Left – Classical Spectrum of HR signal in Figure 7. Right – Power spectrum in % of HF an LF bands by STFT

The low energy values in Figure 9 are also presented in the classical spectrum in Figure 10 at left, and once more only global interpretations are allowed. At right in Figure 10 we present the STFT power of the LF and HF bands in percentage. This plot when compared to the HHT energy variation presents a global similar shape, but by construction (STFT uses a sliding window) only reflects variation between adjacent windows, being this the reason for few irregularities.

The last example of this chapter is obtained using the *101511*[13] criterion as presented in (Fonseca-Pinto et al, 2009; Fonseca-Pinto et al., 2010b)) for the Head-Up-Tilt test. HR and DBP signals plotted are in Figure 11.

[13] This was established for HUT test wit HHT and used 10 heart beats before the tilt manoeuvre and 26 after (in mean 15 during tilt and the rest after).

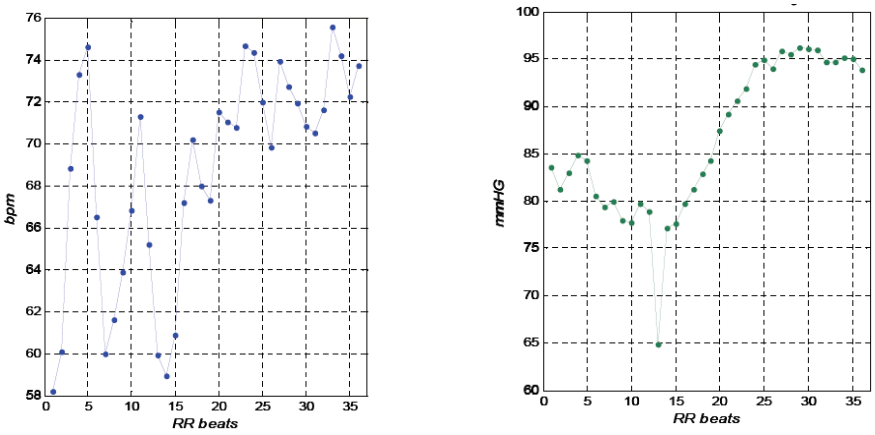

Fig. 11. HR and DBP during 36 heart beats including HUT test

In Figure 12 is possible to observe the instantaneous energy variation obtained by HHT. The increase in DBP after 15th heart beat is conditioned by and sympathetic inflow, and the big variability in HR until 15th heart beat, is captured by the Instantaneous energy representation in Figure 13. In all this period, in which we assist to a contention in HRV (by increasing vagal flow) and then in a preeminent DBP increase (by increase the sympathetic contribution) SVB can be calculated at each heart beat. In fact, this is one of the main differences in using or not interpolation, and by this way, losing time information.

When we assist to a postural change, blood goes to inferior members and to distal parts of superior members. As a result compensatory mechanisms act by increasing sympathetical activity, whose action can be immediate (at the order of seconds) or during hours. When this compensatory mechanisms acts immediately, such regulation must by inferred in beat-to-beat fluctuation, being this the natural scale for getting autonomic regulatory information.

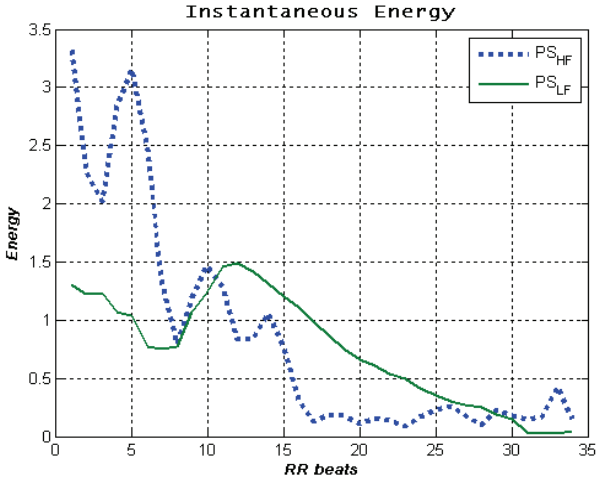

Fig. 12. Instantaneous Energy fluctuation of HF and LF spectrum by HHT

3.2 Lesion border detection and artefact removal in dermoscopic images

Skin cancer is one of the cancer types with most rapidly increasing prevalence and is also one of the most common form of malignancy in humans (Celebi et al., 2007). It is expected that its impact in public health will increase significantly in the coming decades in the absence of effective intervention today (Boyle et al., 2007).

Early detection of skin lesions is critical to prevent this kind of malignancies. Dermatologists use epiluminescence microscopy, or dermatoscopy as is usually called, to perform early diagnosis of melanocytic lesions and to track the progression thereof.

Dermatoscopy uses a polarized light source and a magnifying lens. A fluid is usually spread on the skin surface to minimize light scattering, and thus increase the performance of this technique. The use of this fluid and the presence of hairs, give rise to conspicuous artefacts in dermatoscopic images.

The classification of some melanocytic lesions is sometimes difficult, even for experienced specialists. The lesion border is especially relevant for diagnosis since it allows to gather information about the shape of the lesion, growth path, and growth rate.

The early detention of lesions is crucial to prevent malignancies. Early detection requires periodic monitoring of suspected lesions. Currently dermatologists often resort to digital dermoscopes and computer storage of the information. Computers can also be used to perform automatic lesion border detection. The presence of artefacts may induce artificial borders, thereby jeopardizing the efficiency of automatic detection algorithms (Fonseca-Pinto et al., 2010a)). Artefact removal is a required pre-processing step to improve the quality of detection.

3.2.1 IEMD and image processing

EMD was developed for one-dimensional signals but is possible to extend this procedure to two dimensional arrays. In this work, a 2D extension of EMD is presented, called Image Empirical Mode Decomposition (IEMD). The obtained modes are called 2dIMF's.

An image is an array of pixels that can be treated as a matrix. Each row of this matrix stands for the energy of this set of pixels, and therefore is possible to plot this information. By this way we obtain a one-dimensional signal and it is possible to apply EMD to this one-dimensional signal.

Performing EMD in succession to all rows leads to a set of IMF's for each row, and the set of all IMF's of the same order constitutes a set of 2dIMF's.

Dermoscopic images used in this work are obtained in RGB format and therefore they need to be pre-processed to before application of IEMD. Each image in RGB format corresponds to an array with dimensions $(m, n, 3)$ allowing the extraction of components R, G and B to be individually treated as described above. The final set of 2dIMF's is obtained after each individual matrix processing, by summing up the results. An example of 2dIMF extraction by IEMD from a dermoscopic image is presented in Figure 14.

Dermoscopic images involve some artefacts directly related to this kind of images, i.e. hairs and air bubbles. The correct outline of lesion borders is critical for diagnosis, and the efficiency of automatic lesion border detection is hampered by artefacts.

Artefact removal comprises two steps: 1) detection of corrupted pixels, and 2) assignment of new intensity value associated to those pixels, while trying to minimize changes in the relevant image features.

The above presented IEMD decomposition is used in this work to detect artefacts. Figure 14 suggests that 2dIMF's capture the main visible artefacts.

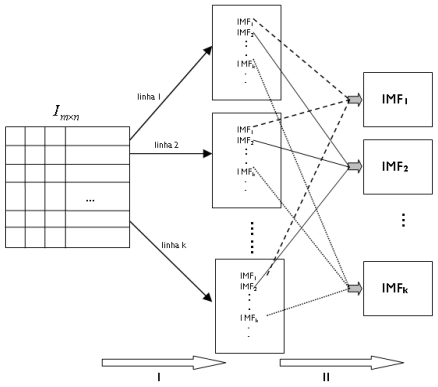

Fig. 13. IEMD extraction from the original matrix

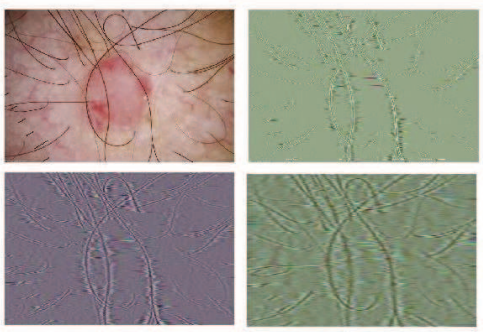

Fig. 14. Dermoscopic image (top left), 2dIMF1 (top right), 2dIMF2 and 3 (bottom images)

3.2.2 Artefact removal by IEMD

Air bubbles and hairs represent bursts of high frequency oscillation that are efficiently captured by the firsts 2dIMF's. These high variation regions are enhanced by applying the following algorithm to 2dIMF1 presented in Figure 16.

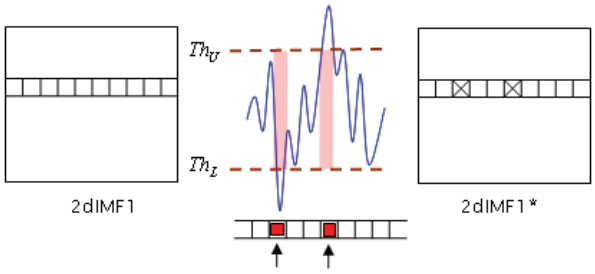

Fig. 15. Detection of anomalous pixels in 2dIMF1

After IEMD we get the first component (2dIMF1, with dimensions $r \times c$) and the maximum (M) and minimum (m) energy value is calculated

$$M = \max_{\substack{i=1,\ldots,r \\ j=1,\ldots,c}} \{2dIMF1(i,j)\}; \quad m = \min_{\substack{i=1,\ldots,r \\ j=1,\ldots,c}} \{2dIMF1(i,j)\} \tag{17}$$

and the inner variation is calculated by $R = M + |m|$.
Using this inner variation above defined we set an empirically chosen threshold range. This threshold range is symmetric and the *Th* of Figure 15 is calculated by $Th = R \times h$, resulting in a percentage of the inner variation characterized by the h value as defined by the user for each image component.
After this step the reassignment of anomalous pixels can be made using several strategies. In this work we chose a simple approach that consists of averaging the values of neighbouring, non-artefact pixels.
This IEMD procedure amounts in fact to filtering. However, contrary to common filter procedures, this technique targets only those pixels where artefacts exist, leaving the remaining image unchanged. It is not a blind procedure, but rather an adaptative and oriented strategy to remove artefacts in dermoscopic images.
As stated in the beginning, automatic border detection is important to improve early diagnosis and the presence of artefacts decreases the efficiency of lesion border detection (specifically, the presence of hairs induces artificial lesion borders). Common filters (in this case low pass filters) applied to these images tend to mask those artefacts, and have the disadvantage of decreasing image resolution. Besides, they tend to blur important diagnosis features such as pigmented networks and blue-white zones.
Dermoscopic images used as examples were obtained from the database of the skin cancer society of Australia in *www.dermoscopyatlas.com* . Low pass filtering used as a comparative model was created with *imfilter.m* function from Matlab using symmetric boundary options.

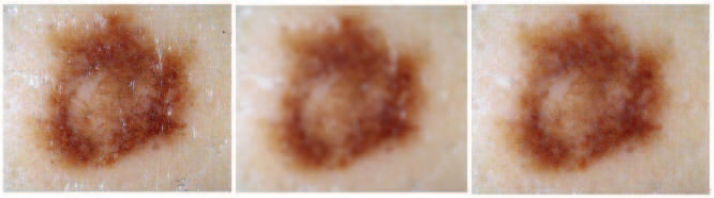

Fig. 16. Dermoscopic image with air bubbles (left), image after classical low pass filtering (middle) and image after IEMD filtering

The performance of IEMD artifact removal is illustrated in Figure 16 in which a dermoscopic image of a melanoma is presented. In this case it is possible to detect several air bubbles due to fluid application on the skin. The image after classical low pass filtering (in the middle) presents poor resolution. The image after IEMD artifact removal (right) indicates a clearly better performance in terms of image resolution preservation.

3.2.3 IEMD as a filter in automatic border lesion detection

After the IEMD artefact removal, we use *bwtraceboundary.m* from the Matlab™ signal processing toolbox to detect border lesions. In the present work we compare the

performance of this routine applied to the original dermoscopic image (original), to the image filtered by a classical low pass filter (classical filter) and to the image after being submitted to IEMD (IEMD filter).

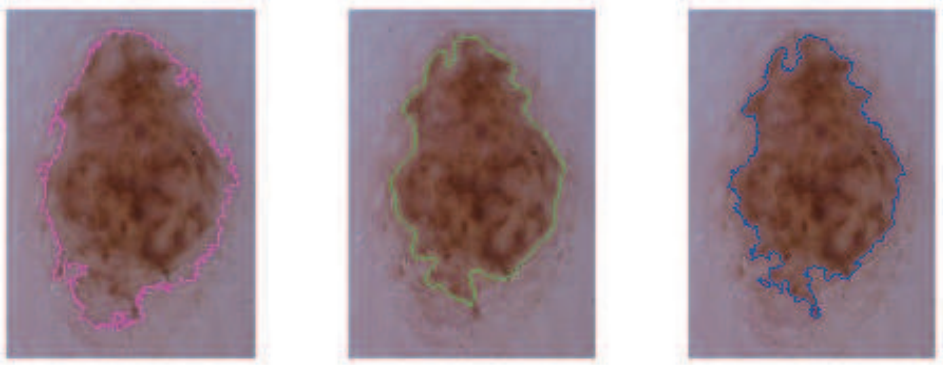

Fig. 17. Automatic border detection without filtering (left), with classical filter (middle) and with IEMD filter (right)

The first example presented in Figure 17 is an *acral melanocytic naevus*. In this case air bubbles are presented and as expected they corrupt the efficiency of automatic border detection, as can be seen in Figure 17 on the left. The two filtering schemes (classical and IEMD) are presented at the same figure at the centre and right. Selective filtering, in this case, resulted in improved border detection (notice the small lesion area at the bottom, missed by classical filtering approach and detected by IEMD).
In the second example, presented in Figure 18, both main artefact sources (air bubbles and hairs) are present, resulting in a tough challenge for the artefact removal algorithm.

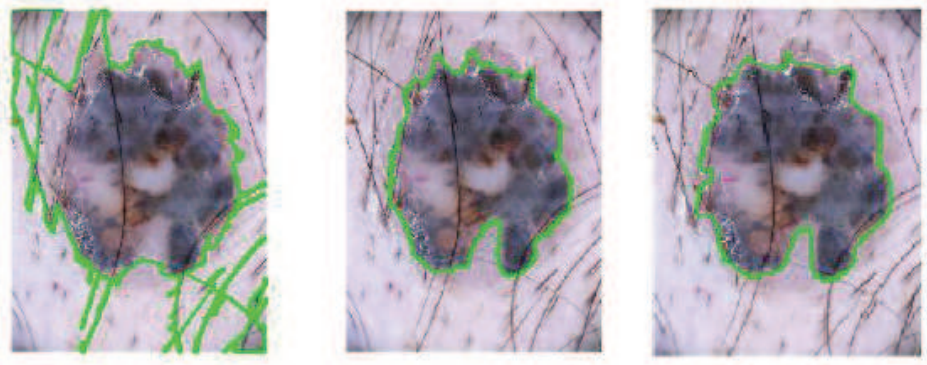

Fig. 18. Automatic border detection without filtering (left), with classical filter (middle) and with IEMD filter (right)

As expected, the automatic border detection of this image without any kind of filtering leads to nonsense results and produces artificial borders in the lesion like those presented in Figure 18 at left. After filtering, it is possible to see that both filtering schemes produce

much more reasonably looking borders. Classical filtering leads to soft borders, as opposed to IEMD, where the lesion outline seems to be more realistic.
We present in Figure 19 another example of automatic border detection. This is a melanocytic lesion melanoma *acral lentiginous* and in this case only air bubbles are present. After lesion border automatic detection it is possible to see that, again, IEMD leads to a more detailed outline of the border, as opposed to the softer border yielded by classical filtering, due to the filter-induced blurring.

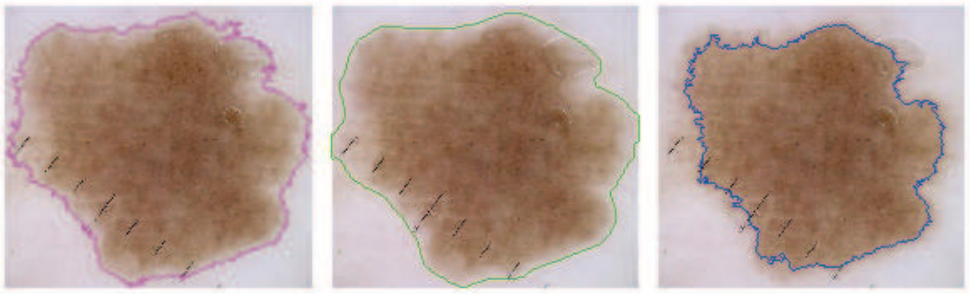

Fig. 19. Automatic border detection without filtering (left), with classical filter (middle) and with IEMD filter (right)

4. Conclusion

The way we have to access to information from systems is, sometimes enrolled in complicated schemes and finally what we get is more a function of the process and less a function of the true phenomenon. In fact, a truly data processing technique must be designed in order to let the data talk! As we have seen, hinders related with stationarity and linearity may cause constrains, when they are overlooked.
To find solutions to old problems, new strategies must be used, as is the case in the EMD decomposition, scratching with traditional an *a priori* basis assumption. In this specific case, as long as whole methodology were empirical and without an analytical formulation, we have to face results with some prudence, filtered by a stable theoretical knowledge in signal processing, allowing to use those results with tranquillity.
People who work with this technique always sited Heaviside, an English Mathematician how said in other context
"Shall I refuse my dinner because I do not fully understand the process of digestion?"

5. Acknowledgements

This Chapter reflects part of the work done during my PhD in the Institute of Biophysics and Biomedical Engineering (IBEB) at the Faculty of Sciences in Lisbon, hence I whish to thank my supervisor Professor Alexandre Andrade.
Data for testing the methodology to access to SVB was obtained in the Laboratory of Autonomic Nervous System at the Hospital de Santa Maria em Lisbon. I want to thank for the data and also for all support from Professor José Luis Ducla-Soares and is team.

6. References

Addison P (2002), *The Ilustrated Wavelet Transform Handbook*, Institute of Physics, ISBN 0750306920.

Auger F, Flandrin P, Gonçalvès P, Lemoine O. *Time frequency toolbox for Matlab*, Freeware at URL (http://tftb.nongnu.org). Accessed 24 May 2009.

Akselrod S, Gordon D, Madwed JB, Snidman NC, Shannon DC, Cohen RJ(1985), Hemodynamic regulation: Investigation by spectral analysis, *Am. J. Physiol*. 18, H867-H875

Boashash B (1992), Estimate and interpreting the instantaneous frequency of a signal: I – Fundamentals, *Proc IEEE* 80, 520-538.

Carvalho JLA, Rocha A, Junqueira L, Souza Neto J, Santos I, Nascimento F (2003); A tool for Time-frequency analysis of heart rate variability, *Proceedings of the 25th annual International Conference of the IEEE EMBC*, 2574-2577.

Caseiro P, Fonseca-Pinto R, Andrade A, Screening of Obstructive Sleep Apnea using Hilbert-Huang Decomposition of Oronasal Airway Pressure recordings, *Medical Engineering and Physics*, 2010.

Cohen L (1995), *Time-Frequency Analysis*. Prentice-Hall,. Englewood Clis, NJ, 1995

Daubechies I (1992), *Discrete Wavelet Transform: Frames*, Chap III of X Lectures on Wavelets. Capital City Press, pp 53-106.

Daubechies I. (1988). Orthonormal Bases of Compactly Supported Wavelets, *Comm. Pure Applied Math*., Vol 41, pp. 906-966.

Ding H, Huang Z, Song Z, Yan Y (2007) Hilbert–Huang transform based signal analysis for the characterization of gas–liquid two phase flow; *Flow measurement and instrumentation*:18, 37-46.

Ducla-Soares J L, Santos-Bento M, Laranjo S, Andrade, A, Ducla-Soares E, Boto J P, Silva-Carvalho L, Rocha I. (2007). Wavelet analysis of autonomic outflow of normal subjects on head-up tilt, cold press test, valsalva manoeuvre and deep breathing, *Journal of Experimental Physiology*, 92, 677-687.

Eckberg DL. (1997). Sympathovagal balance: a critical appraisal. *Circulation 96*, 3224-3232.

Flandrin P, Gonçalvès P, Rilling G. (2004), Empirical Mode Decomposition as a filter bank, *IEEE Signal Processing Letters*, Vol XI .

Fonseca-Pinto R, Ducla-Soares J. L, Araújo F, Aguiar P, Andrade A (2009), On the influence of time-series length in EMD to extract frequency content: Simulations and models in biomedical signals, *Medical Engineering & Physics* 31 713–719.

Fonseca-Pinto R, Caseiro P, A. Andrade (2010a)), Bi-dimensional Empirical Mode Decomposition (BEMD) in dermoscopic images: artefact removal and border lesion detection; *Proceedings of the 7th IASTED international Conference Signal Processing, Pattern recognition and Application*s; 341-345

Fonseca-Pinto R , Andrade A , Araújo F, Aguiar P, Ducla-Soares J.L (2010b)), Access to Sympathovagal Balance (SVB) using Hilbert-Huang Transform (HHT), *Proceedings of the Matemathical Methods in Engineering conference 2010, MME2010*.

Freeman R. (1997). *Non invasive evaluation of heart rate variation. The time domain. Clinical Autonomic Disorders* (2nd edition) Philadelphia, Lippincott-Raven Publishers : 297-307.

Gabor D, Theory of communication, (1993) *IEEE J. Comm. Eng.* 93: 429-457.

Huang N.E, Shen Z, Long SR, Wu MC, Shih HH, Zheng Q, Yen N-C, Tung CC, Liu HH (1998), The Empirical mode decomposition and the Hilbert spectrum for nonlinear and nonstationary time-series analysis. *Proc R Soc Lond A* 454: 903-995.

Huang N, Wu M, Qu W, Long S, Shen S. (2003), Applications of Hilbert-Huang transform to non-stationary financial time series analysis; *Applied stochastic models in business and industry* – Vol 19, 245-268.

Joyner M, Shepherd J. (1997). *Autonomic regulation of circulation: Clinical Autonomic Disorders* (2nd edition) Philadelphia, Lippincott-Raven Publishers : 61-71.

Long S R, Huang N E, Tung C C, Wu M L, Lin R Q, Mollo-Christensen, E &Yuan Y. (1995), The Hilbert techniques: an alternate approach for non-steady time series analysis. *IEEE Geoscience Remote Sensing Soc.* Lett. 3, 6-11.

Malik M. (1996), Heart rate variability: Standards of measurement, physiological interpretation, and clinical use, Task Force of The European Society of Cardiology and The North American Society of Pacing and Electrophysiology, *European Heart Journal* 17, 354-381.

Malliani A, Pagani M, Lombardi F, Cerutti D. (1991). Cardiovascular neural regulation explored in the frequency domain, *Circulation,* 84, 482 – 492.

Meyer Y. (1993). Wavelets: Algorithms and Applications, *Society for Industrial and Applied Mathematics*, Philadelphia, pp. 13-31, 101-105.

Parati G, Saul J.P, Di Rienzo M, Mancia G. (1995). Spectral analysis of blood pressure and heart rate variability in evaluating cardiovascular – A critical appraisal, *Hypertension,* 25, pp 1276-1286.

Quek T, Tua S, Wang Q. (2003), Detecting anomalies in beams and plate based on the Hilbert-Huang transform of real signals; *Smart materials and structures*- vol12 , 447-460.

Rao R, Hsu E-C (2008) Hilbert-Huang Transform Analysis Of Hydrological And Environmental Time Series; *Water Science and Technology Library*-vol 60.

Rilling G., Flandrin P., Gonçalves P. (2003), On Empirical Mode Decomposition and its Algorithms, *IEEE-EURASIP Workshop on Nonlinear Signal and Image Processing NSIP-03*, Grado (Italy). URL code in:
http://perso.ens-lyon.fr/patrick.flandrin/emd.html.

Salisbury J, Sun Y(2007). Rapid screening test for sleep apnea using a nonlinear and nonstationary signal processing technique; *Medical Engineering & Physics*, 29(3):336-43.

Shepherd R, Shepherd J. (1988). *Control of blood pressure and the circulation in man, Autonomic Failure: A textbook of clinical disorders of the autonomic nervous system* (2nd edition) ,Oxford, Oxford University Press,:80-96.

Sleight P, Casadei B. (1995). *Relationships between heart rate, respiration and blood pressure variabilities, Hear rate variability*. Armonk, NY. Futura Publishing Company : 311-327.

Tang J, Zou Q. Tang Y, Liu B, Zhang Xiao-kai (2007) Hilbert-Huang Transform for ECG De-Noising; *Bioinformatics and Biomedical Engineering*, 664-667.

Xun J, Yan S (2008). A revised Hilbert–Huang transformation based on the neural networks and its application in vibration signal analysis of a deployable structure; *Mechanical Systems and signal processing*-Vol 22, 1705-1723.

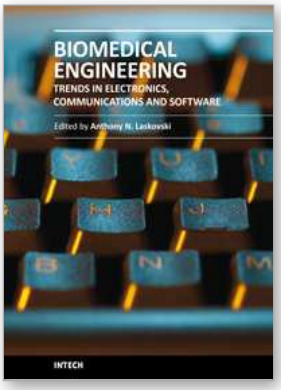

Biomedical Engineering, Trends in Electronics, Communications and Software

Edited by Mr Anthony Laskovski

ISBN 978-953-307-475-7
Hard cover, 736 pages
Publisher InTech
Published online 08, January, 2011
Published in print edition January, 2011

Rapid technological developments in the last century have brought the field of biomedical engineering into a totally new realm. Breakthroughs in materials science, imaging, electronics and, more recently, the information age have improved our understanding of the human body. As a result, the field of biomedical engineering is thriving, with innovations that aim to improve the quality and reduce the cost of medical care. This book is the first in a series of three that will present recent trends in biomedical engineering, with a particular focus on applications in electronics and communications. More specifically: wireless monitoring, sensors, medical imaging and the management of medical information are covered, among other subjects.

How to reference

In order to correctly reference this scholarly work, feel free to copy and paste the following:

Rui Fonseca-Pinto (2011). A New Tool for Nonstationary and Nonlinear Signals: The Hilbert-Huang Transform in Biomedical Applications, Biomedical Engineering, Trends in Electronics, Communications and Software, Mr Anthony Laskovski (Ed.), ISBN: 978-953-307-475-7, InTech, Available from: http://www.intechopen.com/books/biomedical-engineering-trends-in-electronics-communications-and-software/a-new-tool-for-nonstationary-and-nonlinear-signals-the-hilbert-huang-transform-in-biomedical-applica

INTECH
open science | open minds

InTech Europe
University Campus STeP Ri
Slavka Krautzeka 83/A
51000 Rijeka, Croatia
Phone: +385 (51) 770 447
Fax: +385 (51) 686 166
www.intechopen.com

InTech China
Unit 405, Office Block, Hotel Equatorial Shanghai
No.65, Yan An Road (West), Shanghai, 200040, China
中国上海市延安西路65号上海国际贵都大饭店办公楼405单元
Phone: +86-21-62489820
Fax: +86-21-62489821